Chapter 3. Formation and Reactivity of Dinuclear Complexes with Coordinated Disulfide Bond

3-1. Introduction

As described in chapter 1, the facial-type mononuclear complexes, *fac(S)*-$[M(aet)_3]$ ($M = Co^{III}$, Rh^{III}, and Ir^{III}) can function as the building blocks of the tridentate ligands and form a variety of S-bridged polynuclear complexes.[1-9] Moreover, the H_2O_2 oxidation of the thiolato group coordinated to the metal ion in the *fac(S)*-$[M(aet)_3]$ ($M = Co^{III}$ and Rh^{III}) has been given the mononuclear sulfenato or sulfinato complexes, *fac(S)*-$[M(aese)_n(aesi)_{3-n}]$ ($n = 0 - 3$).[10,11] In chapter 2, the iridium complex **3**, which does not involve chromium(III) ion, besides the S-bridged trinuclear complexes, $[Cr\{Ir(aet)_3\}_2]^{3+}$, were simultaneously obtained in the reaction of *fac(S)*-$[Ir(aet)_3]$ with chromium(III) nitrate.[1] It can be considered that the oxidation of *fac(S)*-$[Ir(aet)_3]$ was caused by the lability of Cr-S bonds in acid condition. Further, the equivalent oxidation on the thiolato group of mononuclear complexes (e. g. $[Co(aet)(en)_2]^{2+}$) may form a coordinated disulfide bond, which connects two metal centers to give a dinuclear complexes (e. g. $[Co_2(en)_4(cysta)]^{6+}$).[12] Such complexes would be of interest in the electrochemistry related to reactivity of the disulfide bond, because of the importance of thiol-disulfide couple in biological systems, such as disulfurization catalysis.[13,14]

Equivalent oxidation reactions of the mononuclear thiolato cobalt(III) complexes have been attempted, but the dinuclear complexes with a coordinated disulfide bond has little been isolated because of the concomitant cleavage of the M-S bond.[14-16] For example, it has been shown that the oxidation reaction of $[Co(aet)(en)_2]^{2+}$ with neptunium(VI) in acid produces the mononuclear disulfide complex, $[Co(Hcysta\text{-}N,S)(en)_2]^{4+}$, via the dinuclear intermediate with the bridged cysta ligand.[15] The oxidation reaction of *fac(S)*-$[Co(aet)_3]$ with HNO_3 results in the isolation of the S-bridged tricobalt(III) complex, $[Co\{Co(aet)_3\}_2]^{3+}$, accompanied by the release of free

cystamine.[16] In these reactions, the mononuclear disulfide complex, $[Co(Hcysta\text{-}N,S)(en)_2]^{4+}$, or the tricobalt(III) complex, $[Co\{Co(aet)_3\}_2]^{3+}$, cannot be formed without the cleavage of the M-S bond. It has been known that the M-S bonds of the iridium(III) or rhodium(III) complexes are stronger than those of the cobalt(III) complexes. Accordingly, it seems that the dissociation of the aet ligands are inhibited and the intended dinuclear complex with the disulfide bond can be obtained by the use of the iridium(III) or rhodium(III) complexes with the sulfur donor atoms, if it prevents ligands from dissociating

In this chapter, I attempted to prepare the dinuclear complexes with a bridging disulfide bond *via* equivalent oxidation of *fac(S)*-$[M(aet)_3]$ ($M = Ir^{III}$ and Rh^{III}). I have found that fairly stable dinuclear complexes, $[M_2(aet)_4(cysta)]^{2+}$ ($M = Ir^{III}$ (3), Rh^{III} (4)), using various oxidation reagents. Each crystal structure of the complexes **3** and **4** was determined by the X-ray diffraction study and the stereochemical, spectrochemical, and electrochemical properties of the present complexes was discussed. The reactivity of mononuclear *fac(S)*-$[M(aet)_3]$ were investigated, and the difference between iridium(III) and rhodium(III) complexes was observed well. Formation of the dinuclear complex, $[Ir_2(aet)_4(cysta)]^{2+}$ (3), by the decomposition of the trinuclear complex, $\Delta\Lambda$-$[Cr^{III}\{Ir(aet)_3\}_2]^{3+}$ (1a), as well as the reactivity of the dinuclear complexes are also explored.

3-2. Experimental

3-2-1. Materials

All chemicals were purchased from the companies as described in chapter 2. They were of reagent grade, and were used without further purification.

3-2-2. Preparation of Complexes

fac(S)-$[Ir(aet)_3]$, *fac(S)*-$[Rh(aet)_3]$, *fac(S)*-$[Co(aet)_3]$, and *fac(S)*-

$[Cr(aet)_3]$ These complexes were prepared by the methods described in chapter 2.

fac(S)-$[Ir(L\text{-}cys\text{-}N,S)_3]^{3-}$ and *fac(S)*-$[Rh(L\text{-}cys\text{-}N,S)_3]^{3-}$ These complexes were prepared by the methods described in the literatures.[2-4,17]

$[Ir_2(aet)_4(cysta)]^{2+}$ (3) *Method A:* *fac(S)*-$[Ir(aet)_3]$ (0.30 g, 0.71 mmol) was dissolved in 10 cm^3 of 1 mol dm^{-3} HCl, and the pale brown solution was stirred at 60 °C for 15 min, whereupon it became a dark orange solution. To this solution was added 1 cm^3 of a saturated NaCl solution, followed by standing at room temperature for 1 d. The resulting dark orange crystals ($3Cl_2 \cdot 4H_2O$) were collected by filtration. A second crop of the product was collected by standing the mother liquor at room temperature for a few days. Single crystals suitable for X-ray analysis were obtained by recrystallization from ca. 0.05 mol dm^{-3} chromium(III) chloride aqueous solution at room temperature. Similar crystals were also obtained by the reaction under nitrogen atmosphere. Yield: 0.16 g (46 %). Found: C, 14.55; H, 4.41; N, 8.40 %. Calcd for $[Ir_2(aet)_4(cysta)]Cl_2 \cdot 4H_2O$ = $C_{12}H_{36}N_6S_6Cl_2Ir_2 \cdot 4H_2O$: C, 14.64; H, 4.51; N, 8.54 %.

Method B: To a suspension containing *fac(S)*-$[Ir(aet)_3]$ (0.10 g, 0.24 mmol) in 2 cm^3 of water was added $Ce(SO_4)_2 \cdot 4H_2O$ (0.10 g, 0.25 mmol). After the mixture had been stirred at room temperature for 30 min, the resulting brown powder ($3SO_4$) was collected by filtration. The counter anion was exchanged by adding this powder into 5 cm^3 of a saturated $NaNO_3$ solution at 40 °C for 10 min. The resulting brown powder ($3(NO_3)_2 \cdot 3.5H_2O$) was recrystallized from warm water by adding a few drops of a saturated $NaNO_3$ solution. Yield: 0.074 g (61 %). Found: C, 14.02; H, 4.15; N, 10.79; Ir, 37.97 %. Calcd for $[Ir_2(aet)_4(cysta)](NO_3)_2 \cdot 3.5H_2O$ = $C_{12}H_{36}N_8O_6S_6Ir_2 \cdot 3.5H_2O$: C, 14.02; H, 4.21; N, 10.90; Ir, 37.38 %.

Method C: *fac(S)*-$[Ir(aet)_3]$ (0.10 g, 0.24 mmol) was dissolved in 6 cm^3 of 0.15 mol dm^{-3} HNO_3, and the pale brown solution was stirred at 60 °C for 4 h, whereupon it became a dark orange solution. To this solution was added 1 cm^3 of a saturated $NaNO_3$ solution, followed by standing at room temperature for 1 d. The resulting dark orange crystals ($3(NO_3)_2 \cdot 3.5H_2O$)

were collected by filtration. Yield: 0.058 g (48 %).

Method D: To a suspension containing *fac(S)*-[Ir(aet)$_3$] (0.25 g, 0.59 mmol) in 15 cm^3 of water was added Cr(NO$_3$)$_3$·9H$_2$O (1.0 g, 2.5 mmol) in 15 cm^3 of water. The mixture was stirred at 60 °C for 2.5 h, whereupon it became a dark brown solution. After the solution had been stood at room temperature for 1 d, the resulting dark orange crystals (**3**(NO$_3$)$_2$·3.5H$_2$O) were collected by filtration. To this mother liquor was added 5 cm^3 of a saturated NaNO$_3$ solution, followed by standing at room temperature for 3 d. This second crop was collected by filtration. Yield: 0.15 g (49 %).

[Rh$_2$(aet)$_4$(cysta)]$^{2+}$ (4) *Method A:* *fac(S)*-[Rh(aet)$_3$] (0.30 g, 0.91 mmol) was dissolved in 10 cm^3 of 1 mol dm^{-3} HCl. To the yellow solution was added K$_2$Cr$_2$O$_7$ (0.047 g, 0.16 mmol). The mixture was stirred at room temperature for 15 min, whereupon it became a dark orange solution. To this solution was added 1 cm^3 of a saturated NaCl solution, followed by standing at room temperature for 1 d. The resulting dark orange crystals (**4**Cl$_2$·2H$_2$O) were collected by filtration, and one of the crystals was used for X-ray structural analysis. Yield: 0.099 g (28 %). Found: C, 18.52; H, 5.25; N, 10.65 %. Calcd for [Rh$_2$(aet)$_4$(cysta)]Cl$_2$·2H$_2$O = C$_{12}$H$_{36}$N$_6$S$_6$Cl$_2$Rh$_2$·2H$_2$O: C, 18.73; H, 5.24; N, 10.92 %.

Method B: To a suspension containing *fac(S)*-[Rh(aet)$_3$] (0.10 g, 0.30 mmol) in 2 cm^3 of water was added Ce(SO$_4$)$_2$·4H$_2$O (0.13 g, 0.31 mmol). After the mixture had been stirred at room temperature for 1 h, the resulting orange powder (**4**SO$_4$) was collected by filtration. The counter anion was exchanged by adding this powder into 5 cm^3 of a saturated NaNO$_3$ solution at 40 °C for 10 min. The resulting orange powder (**4**(NO$_3$)$_2$·2H$_2$O) was recrystallized from warm water by adding a few drops of a saturated NaNO$_3$ solution. Yield: 0.052 g (42 %). Found: C, 17.36; H, 4.82; N, 13.55; Rh, 23.60 %. Calcd for [Rh$_2$(aet)$_4$(cysta)](NO$_3$)$_2$·2H$_2$O = C$_{12}$H$_{36}$N$_8$O$_6$S$_6$Rh$_2$·2H$_2$O: C, 17.52; H, 4.90; N, 13.62; Rh, 25.02 %.

***fac(S)*-[Ir(aesi)$_3$]** *fac(S)*-[Ir(aet)$_3$] (0.100 g, 0.238 mmol) was dissolved in 3.5 cm^3 of 1 mol dm^{-3} HNO$_3$. To the pale brown solution was added 1 cm^3 of 30 % H$_2$O$_2$, whereupon it became a colorless solution. The

solution was stood at room temperature for 12 h. The resulting white micro crystals were collected by filtration, and washed with ethanol. Yield: 0.110 g (87 %). Found: C, 13.61; H, 3.75; N, 7.94 %. Calcd for $[Ir(aesi)_3]\cdot 0.75H_2O = C_6H_{18}N_3O_6S_3Ir\cdot 0.75H_2O$: C, 13.59; H, 3.71; N, 7.93 %.

fac(S)-**[Rh(aesi)$_3$]** *fac(S)*-$[Rh(aet)_3]$ (0.100 g, 0.302 mmol) was dissolved in 3.5 cm^3 of 1 mol dm^{-3} HNO_3. To the yellow solution was added 1 cm^3 of 30 % H_2O_2, whereupon it became a colorless solution. The solution was stood at room temperature for 12 h. The resulting white micro crystals were collected by filtration, and washed with ethanol. Yield: 0.125 g (94 %). Found: C, 16.26; H, 4.47; N, 9.53 %. Calcd for $[Rh(aesi)_3]\cdot 0.75H_2O = C_6H_{18}N_3O_6S_3Rh\cdot 0.75H_2O$: C, 16.35; H, 4.46; N, 9.53 %.

3-2-3. Measurements

The electronic absorption spectra were recorded with a JASCO V-560 spectrophotometer. All the measurements were carried out in aqueous solution at room temperature. The elemental analyses (C, H, N) were performed by the Analysis Center of the University of Tsukuba. The concentrations of Ir and Rh in the complexes were determined with a NIPPON Jarrell-Ash ICPA-575 ICP spectrophotometer. The diffuse reflectance spectra were recorded with a JASCO V-570 spectrophotometer. The infrared spectra were recorded as a KBr disk with a JASCO FT/IR-550 spectrometer. The Raman spectra were recorded on a JASCO R-800 laser Raman spectrophotometer with an excitation by Ar^+ ion laser line, 514.5 nm, and the samples were in the form of a KBr disk. The ^{13}C NMR spectra (125.759 MHz) were recorded with a BRUKER AM-500 NMR spectrometer in D_2O. The sodium 4,4-dimethyl-4-silapentane-1-sulfonate (DSS) was used as an internal reference. The molar conductances of the complexes were measured with a HORIBA conductivity meter DS-14 in aqueous solution at room temperature. Electrochemical measurements were made by CV-1B apparatus (Biochemical Analytical Systems, Inc. (BAS)) using a glassy-carbon working electrode (BAS, GCE). An aqueous Ag/AgCl/NaCl (3 mol dm^{-3}) electrode (BAS, RE-1) and platinum wire were used as reference and

auxiliary electrodes, respectively. Electrochemical experiments were conducted in a 0.1 mol dm^{-3} sodium sulfate aqueous solution as the supporting electrolyte and the complex concentrations of 1.0 mmol dm^{-3}. Molecular Mechanics calculations (MM2 program) were performed on a Power Macintosh computer with CAChe program.[18]

The changes with time were carried out by the absorption spectral measurements and the column chromatographic technique. A solution containing 0.02 g of *meso*-$[Cr\{Ir(aet)_3\}_2](NO_3)_3 \cdot 3H_2O$ ($\mathbf{1a}(NO_3)_3 \cdot 3H_2O$) in 25 cm^3 of 1 mol dm^{-3} HCl solution was maintained at 40 °C for a definite time. Using 5 cm^3 of these solutions, which was diluted to 25 cm^3 by a 1 mol dm^{-3} HCl solution, the absorption spectral changes with time were measured on a JASCO V-560 spectrophotometer. Another solution of 20 cm^3 was poured onto the SP-Sephadex C-25 column and eluted by a 1 mol dm^{-3} NaCl aqueous solution. Each eluate was diluted to 100 cm^3 and its concentration was measured on a JASCO V-560 spectrophotometer.

3-2-4. Crystallography

Single crystals of $3Cl_2 \cdot 4H_2O$ and $4Cl_2 \cdot 2H_2O$ were used for data collection on a Rigaku AFC-7S four-circle diffractometer with graphite-monochromatized Mo $K\alpha$ (0.71069 Å) radiation. Unit cell parameters were determined by least-squares refinements of 25 reflections ($14.8 < \theta < 15$ °). Crystallographic data and experimental parameters are summarized in Table 3-1. The intensity data were collected by the ω - 2θ scan technique, and the scan rate varied from 1 to 5 ° min^{-1} (on ω). The intensities were corrected for Lorentz and polarization. An empirical absorption correction based on a series of ψ scans was applied. The independent reflections with $I_0 > 1.5\sigma(I_0)$ were used for the structural determinations. The positions of the Ir, Rh, and other atoms were determined by the direct method (SIR92).[19] The difference Fourier maps based on these atomic positions revealed some remaining non-hydrogen atoms. The structures were refined by full-matrix least-squares refinements on F of the positional parameters and the anisotropic thermal parameters of the non-hydrogen atoms in $3Cl_2 \cdot 4H_2O$ or $4Cl_2 \cdot 2H_2O$. The

Table 3-1. Crystallographic Data for $[Ir_2(aet)_4(cysta)]Cl_2 \cdot 4H_2O$ ($3Cl_2 \cdot 4H_2O$) and $[Rh_2(aet)_4(cysta)]Cl_2 \cdot 2H_2O$ ($4Cl_2 \cdot 2H_2O$)

	3	4
Formula	$C_{12}H_{44}N_6O_4S_6Cl_2Ir_2$	$C_{12}H_{40}N_6O_2S_6Cl_2Rh_2$
Formula weight	984.22	769.56
Cryst. dimems. / mm	0.50 x 0.25 x 0.23	0.45 x 0.40 x 0.08
Cryst. System	Monoclinic	Monoclinic
Space group	$P2_1/a$ (No. 14)	$P2_1/c$ (No. 14)
a / Å	12.427(2)	11.788(2)
b / Å	8.879(1)	8.485(1)
c / Å	13.387(1)	14.800(2)
β / °	91.947(10)	112.980(9)
V / Å^3	1476.3(3)	1362.9(3)
Z	2	2
D_{calcd} / g cm^{-3}	2.214	1.875
μ(Mo $K\alpha$) / cm^{-1}	96.65	18.86
Transm. Coeff.	0.4644 - 0.9988	0.7076 - 0.9986
Temp / K	296	296
No. of measd reflcns	3619	3342
No. of reflcns for used	3159 ($I_0 > 1.5\sigma(I_0)$)	2872 ($I_0 > 1.5\sigma(I_0)$)
No. of parameters	146	137
Final R	0.031	0.023
Final R_w	0.052	0.048
GOF	1.46	1.35

Table 3-2. Final Atomic Coordinates and Equivalent Isotropic Thermal Parameters (B_{eq} / Å^2)[a] for Non-Hydrogen Atoms of $[Ir_2(aet)_4(cysta)]Cl_2 \cdot 4H_2O$ ($3Cl_2 \cdot 4H_2O$)

Atom	x	y	z	B_{eq}
Ir(1)	0.50129(1)	0.11181(2)	0.80269(1)	0.01987(8)
S(1)	0.4475(1)	0.0784(2)	0.96063(10)	0.0242(3)
S(2)	0.6251(1)	0.2955(2)	0.8549(1)	0.0284(3)
S(3)	0.6280(1)	-0.0839(2)	0.8021(1)	0.0312(3)
N(1)	0.3825(4)	-0.0534(6)	0.7591(4)	0.031(1)
N(2)	0.3896(4)	0.2948(6)	0.7892(4)	0.029(1)
N(3)	0.5466(4)	0.1482(6)	0.6550(4)	0.029(1)

Table 3-2. Continued.

Atom	x	y	z	B_{eq}
C(1)	0.3336(5)	-0.0491(8)	0.9374(5)	0.035(2)
C(2)	0.3532(5)	-0.1455(7)	0.8486(5)	0.038(2)
C(3)	0.5422(6)	0.4616(7)	0.8311(6)	0.043(2)
C(4)	0.4260(5)	0.4285(7)	0.8474(5)	0.039(2)
C(5)	0.6800(5)	-0.0543(8)	0.6769(5)	0.035(2)
C(6)	0.5951(5)	0.0124(7)	0.6083(4)	0.032(1)
Cl(1)	0.6737(1)	0.4834(2)	0.5891(1)	0.0491(4)
O(1w)	0.4393(5)	-0.3169(8)	0.6125(5)	0.068(2)
O(2w)	0.3465(4)	0.2675(6)	0.5724(4)	0.051(1)

a) B_{eq} denotes the equivalent isotropic temperature factors, $B_{eq} = (8\pi^2/3)\Sigma\Sigma U_{ij}a^*_i a^*_j a_i \cdot a_j$

Table 3-3. Final Atomic Coordinates and Equivalent Isotropic Thermal Parameters (B_{eq} / Å^2)[a)] for Non-Hydrogen Atoms of $[Rh_2(aet)_4(cysta)]Cl_2 \cdot 2H_2O$ ($4Cl_2 \cdot 2H_2O$)

Atom	x	y	z	B_{eq}
Rh(1)	0.80566(2)	0.35584(2)	0.03946(1)	0.01783(8)
S(1)	0.92268(5)	0.54947(7)	0.01120(4)	0.0219(1)
S(2)	0.92558(7)	0.35268(7)	0.20713(5)	0.0283(2)
S(3)	0.91528(7)	0.15076(7)	0.00878(6)	0.0259(2)
N(1)	0.6966(2)	0.3688(2)	-0.1154(2)	0.0254(5)
N(2)	0.6992(2)	0.5337(3)	0.0765(1)	0.0259(5)
N(3)	0.6950(2)	0.1776(3)	0.0591(2)	0.0260(5)
C(1)	0.8280(2)	0.5900(3)	-0.1169(2)	0.0284(6)
C(2)	0.7662(2)	0.4415(3)	-0.1684(2)	0.0291(6)
C(3)	0.8341(3)	0.4890(4)	0.2478(2)	0.0366(7)
C(4)	0.7742(3)	0.6122(3)	0.1720(2)	0.0337(7)
C(5)	0.8212(3)	-0.0134(3)	0.0164(2)	0.0360(7)
C(6)	0.7609(3)	0.0248(3)	0.0878(2)	0.0345(7)
Cl(1)	0.50951(7)	0.68677(10)	-0.14360(6)	0.0427(2)
O(1w)	0.5126(3)	0.0723(3)	-0.1438(2)	0.0615(8)

a) B_{eq} denotes the equivalent isotropic temperature factors, $B_{eq} = (8\pi^2/3)\Sigma\Sigma U_{ij}a^*_i a^*_j a_i \cdot a_j$

hydrogen atoms on the aet ligands were fixed by the geometrical and thermal constrains (C-H = N-H = 0.95 Å and $U = 1.3U$(C, N)). All the calculations were performed on an Indigo II computer using the teXsan crystallographic software package.[20] The final atomic coordinates for non-hydrogen atoms are given in Tables 3-2 and 3-3.

3-3. Results and Discussion

3-3-1. X-Ray Crystal Structures

X-ray structural analysis for each of the dark orange crystals ($3Cl_2 \cdot 4H_2O$ and $4Cl_2 \cdot 2H_2O$) revealed the presence of a discrete complex cation, two chloride anions, and some water molecules. Perspective drawings of the entire complex cations **3** and **4** are given in Figures 3-1 and 3-2, respectively. The selected bond distances and angles are listed in Table 3-4. As shown in Figures 3-1 and 3-2, the complex cation **3** is isostructural with **4**, that is, **3** and **4** consist of two approximately octahedral *fac(S)*-[$M(aet)_3$] ($M = Ir^{III}$ (**3**), Rh^{III} (**4**)) units, which are linked by one sulfur-sulfur bond (S(1)-S(1)* = 2.158(3) Å for **3**; 2.147(1) Å for **4**). These sulfur-sulfur bond lengths are longer than those of the disulfur complexes (1.98 - 2.10 Å), which have various coordination geometries.[13] In both of the complexes **3** and **4**, a half of the complex cations and two chloride anions are crystallographically independent in the unit-cell. This implies that the entire complex cations are divalent. This is compatible with the observed molar conductivity in water of 208 S cm^2 mol^{-1} for **3** and 227 S cm^2 mol^{-1} for **4**, which are in agreement with those of the 1 : 2 electrolytes, $[Ni^{II}\{M(aet)_3\}_2]^{2+}$ ($M = Co^{III}$ and Rh^{III}) (215 and 220 S cm^2 mol^{-1}, respectively).[21] From these results and the formal charge of the coordinated ligands, it is reasonable to assume that the oxidations occur only at one coordinated thiolato group in the *fac(S)*-[$M(aet)_3$] units to form the disulfide bond, while the iridium or rhodium atom retains the +3 oxidation state.

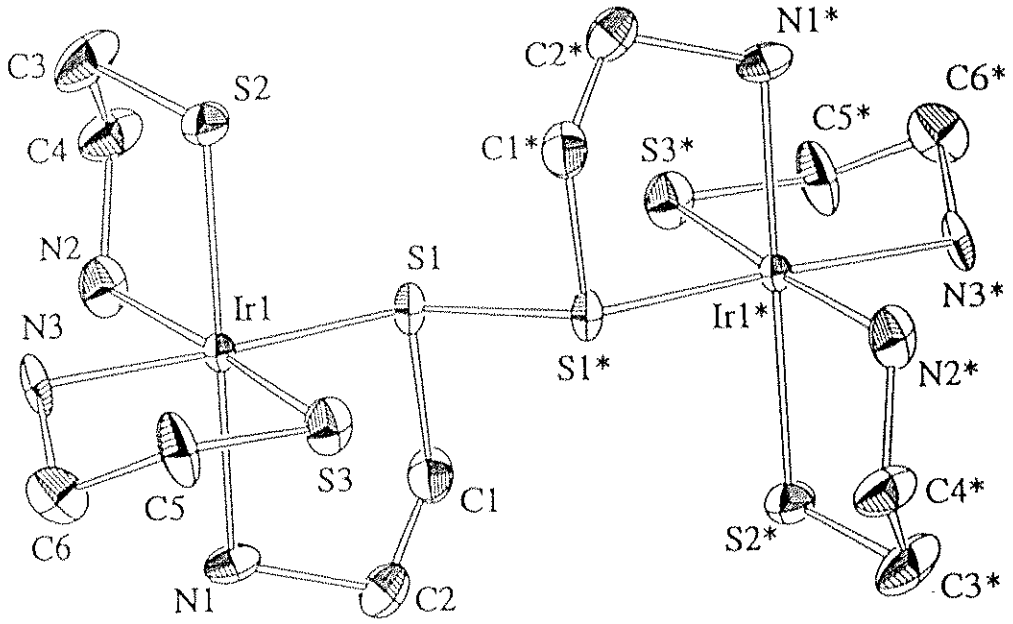

Figure 3-1. Perspective view of $\Delta_R\Lambda_S$-$[Ir_2(aet)_4(cysta)]^{2+}$ (3) with the atomic labeling scheme.

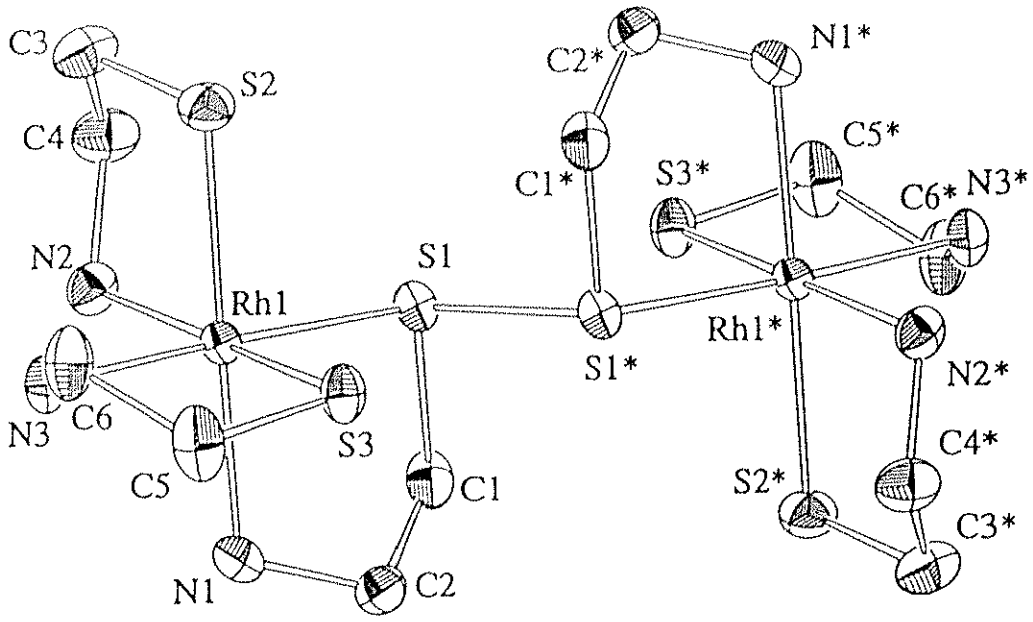

Figure 3-2. Perspective view of $\Delta_R\Lambda_S$-$[Rh_2(aet)_4(cysta)]^{2+}$ (4) with the atomic labeling scheme.

Table 3-4. Selected Bond Distances (Å) and Angles (°) for $[Ir_2(aet)_4(cysta)]^{2+}$ and $[Rh_2(aet)_4(cysta)]^{2+}$

$[Ir_2(aet)_4(cysta)]^{2+}$ (3)		$[Rh_2(aet)_4(cysta)]^{2+}$ (4)	
Ir(1)-S(1)	2.258(1)	Rh(1)-S(1)	2.2865(6)
Ir(1)-S(2)	2.333(1)	Rh(1)-S(2)	2.3276(7)
Ir(1)-S(3)	2.345(1)	Rh(1)-S(3)	2.3157(6)
Ir(1)-N(1)	2.148(5)	Rh(1)-N(1)	2.149(2)
Ir(1)-N(2)	2.141(5)	Rh(1)-N(2)	2.166(2)
Ir(1)-N(3)	2.099(5)	Rh(1)-N(3)	2.090(2)
S(1)-S(1)*	2.158(3)	S(1)-S(1)*	2.147(1)
S(1)-Ir(1)-S(2)	91.42(5)	S(1)-Rh(1)-S(2)	92.56(2)
S(1)-Ir(1)-S(3)	97.22(5)	S(1)-Rh(1)-S(3)	94.67(2)
S(1)-Ir(1)-N(1)	86.7(1)	S(1)-Rh(1)-N(1)	85.42(6)
S(1)-Ir(1)-N(2)	88.1(1)	S(1)-Rh(1)-N(2)	89.78(6)
S(1)-Ir(1)-N(3)	177.9(1)	S(1)-Rh(1)-N(3)	177.67(6)
S(2)-Ir(1)-S(3)	94.76(6)	S(2)-Rh(1)-S(3)	92.71(3)
S(2)-Ir(1)-N(1)	177.5(1)	S(2)-Rh(1)-N(1)	177.66(6)
S(2)-Ir(1)-N(2)	85.1(1)	S(2)-Rh(1)-N(2)	84.76(6)
S(2)-Ir(1)-N(3)	88.8(1)	S(2)-Rh(1)-N(3)	89.73(7)
S(3)-Ir(1)-N(1)	87.0(1)	S(3)-Rh(1)-N(1)	88.65(6)
S(3)-Ir(1)-N(2)	174.7(1)	S(3)-Rh(1)-N(2)	174.97(6)
S(3)-Ir(1)-N(3)	84.8(1)	S(3)-Rh(1)-N(3)	84.82(7)
N(1)-Ir(1)-N(2)	93.3(2)	N(1)-Rh(1)-N(2)	94.03(8)
N(1)-Ir(1)-N(3)	93.1(2)	N(1)-Rh(1)-N(3)	92.29(9)
N(2)-Ir(1)-N(3)	89.9(2)	N(2)-Rh(1)-N(3)	90.81(9)
Ir(1)-S(1)-S(1)*	110.42(9)	Rh(1)-S(1)-S(1)*	110.88(4)

Table 3-5. Structural Energy Calculations (E / kJ mol^{-1}) of $[M_2(aet)_4(cysta)]^{2+}$

	Ir complexes	Rh complexes
$\Delta_R\Delta_R/\Lambda_S\Lambda_S$-isomer	-478.3	-485.5
$\Delta_R\Delta_S/\Lambda_R\Lambda_S$-isomer	-479.6	-488.5
$\Delta_S\Delta_S/\Lambda_R\Lambda_R$-isomer	-474.7	-482.6
$\Delta_R\Lambda_R/\Delta_S\Lambda_S$-isomer	-380.0	-386.2
$\Delta_R\Delta_S$-isomer	-459.9	-468.1
$\Delta_R\Lambda_S$-isomer	-483.3	-491.7

Considering the absolute configurations of the two octahedral *fac(S)*-[M(aet)$_3$] units (Δ and Λ) and the two asymmetric disulfide sulfur atoms (*R* and *S*), ten isomers ($\Delta_R\Delta_R$, $\Lambda_S\Lambda_S$, $\Delta_R\Delta_S$, $\Lambda_R\Lambda_S$, $\Delta_S\Delta_S$, $\Lambda_R\Lambda_R$, $\Delta_R\Lambda_R$, $\Delta_S\Lambda_S$, $\Lambda_R\Delta_S$, and $\Delta_R\Lambda_S$) are possible for $[M_2(aet)_4(cysta)]^{2+}$. The $\Delta_R\Delta_R$, $\Delta_R\Delta_S$, $\Delta_S\Delta_S$, and $\Delta_R\Lambda_R$ isomers and $\Lambda_S\Lambda_S$, $\Lambda_R\Lambda_S$, $\Lambda_R\Lambda_R$, and $\Delta_S\Lambda_S$ isomers are a pair of enantiomers, respectively, which combine to form a racemic compound. The $\Lambda_R\Delta_S$ and $\Delta_R\Lambda_S$ isomers are meso compound. Both of the crystals $3Cl_2\cdot4H_2O$ and $4Cl_2\cdot2H_2O$ contain only meso form with the $\Delta_R\Lambda_S$ configuration, as shown in Figures 3-1 and 3-2. The molecular model examinations reveal that the racemic form exhibits more larger non-bonding interaction between two *fac(S)*-[M(aet)$_3$] units than that of the meso form. The structural energies (MM2 program) were calculated for all of the isomers of $[M_2(aet)_4(cysta)]^{2+}$, and the results are summarized in Table 3-5. The most stable isomer is the $\Delta_R\Lambda_S$ isomer for both iridium and rhodium complexes. Furthermore, when the reaction solutions for $[M_2(aet)_4(cysta)]^{2+}$ were chromatographed on an SP-Sephadex C-25 column, only one orange band was eluted with a 0.15 mol dm^{-3} NaCl aqueous solution. Accordingly, these facts seem to imply that the $\Delta_R\Lambda_S$ isomer is selectively formed by the oxidation reactions for the present disulfide complexes.

The Ir-N(3) distance (2.099(5) Å) in $\Delta_R\Lambda_S$-$[Ir_2(aet)_4(cysta)]^{2+}$ is shorter than the Ir-N(1) (2.148(5) Å) and Ir-N(2) (2.141(5) Å) distances. A similar trend was also observed for the corresponding rhodium complex 4 (Table 3-4). The N(3) atom occupies the *trans* position to the disulfide sulfur atom, while the N(1) and N(2) atoms take the *trans* positions to the thiolato sulfur atoms from aet ligands. Therefore, these seem to depend on the trans influence for the thiolato sulfur atom. This is compatible with the results that the thiolato sulfur atom in $[Co(aet)(en)_2]^{2+}$ exerts a significant trans influence,[22] while the disulfide sulfur atom in $[Co\{NH_2CH_2CH_2S(SCH_2CH_3)$-*N*,*S*$\}(en)_2]^{3+}$ does not.[23] It has been proposed that the presence of trans influence is correlated with the length of the M-S bond, that is, a shorter, stronger M-S bond induces a longer, weaker trans M-N bonds.[14,23] In fact, the Co-S distance (2.272(2) Å) in $[Co\{NH_2CH_2CH_2S(SCH_2CH_3)$-*N*,*S*$\}(en)_2]^{3+}$ is longer than that (2.226(6) Å) in $[Co(aet)(en)_2]^{2+}$.[22,23] However, the M-S(1) distances (M = Ir, 2.258(1)

Å; Rh, 2.2865(6) Å) are shorter than the M-S(2) and M-S(3) distances (Ir, average 2.339(1) Å; Rh, average 2.3217(7) Å). This suggests that the disulfide sulfur atoms are bound to the iridium or rhodium atom more strongly than the thiolato sulfur atoms in $[M_2(aet)_4(cysta)]^{2+}$. This inconsistency may be related to the longer sulfur-sulfur distances of the disulfide bond in $[M_2(aet)_4(cysta)]^{2+}$ (M = Ir, 2.158(3) Å; Rh, 2.147(1) Å). Namely, The stronger M-S(1) bonding enhances back donation from metal ion to π^* orbital of S(1)-S(1)* bond. This trend was also observed for the S-bridged octanuclear complex, $[Cu_4\{Rh(aet)_3\}_2\{Rh_2(aet)_4(cysta)\}]^{6+}$ (2.142(5) Å),[9] are also significantly longer than that (2.033(3) Å) of $[Co\{NH_2CH_2CH_2S(SCH_2CH_3)\text{-}N,S\}(en)_2]^{3+}$.[23]

Most of the bond distances around the iridium atom for $\Delta_R\Lambda_S$-$[Ir_2(aet)_4(cysta)]^{2+}$ are reasonably longer than those around the rhodium atom for $\Delta_R\Lambda_S$-$[Rh_2(aet)_4(cysta)]^{2+}$, considering the covalent radii of the iridium and rhodium metals (Table 3-4). However, the Ir-S(1) (2.258(1) Å) and Ir-N(1) (2.148(5) Å) distances of the cysta ligand for $\Delta_R\Lambda_S$-$[Ir_2(aet)_4(cysta)]^{2+}$ are shorter than those (Rh-S(1), 2.2865(6) Å; Rh-N(1), 2.149(2) Å) for the corresponding rhodium complex (**4**). The bond angles around the iridium atom for **3** are quite similar to those of the rhodium atoms for **4**, except for the S(1)-M-S(3) (Ir, 97.22(5) °; Rh, 94.67(2) °) and S(2)-M-S(3) (Ir, 94.76(6) °; Rh, 92.71(3) °) angles. These suggest that the geometry around the disulfide sulfur atom in $\Delta_R\Lambda_S$-$[Ir_2(aet)_4(cysta)]^{2+}$ is affected by the S-S bond (Table 3-4), whose sulfur atom is bound to the iridium atom more strongly than that to the rhodium atom in the corresponding rhodium complex. As shown in Figures 3-1 and 3-2, furthermore, the S(3)-N(3) chelate rings are the parallel conformations (λ for Δ_R; δ for Λ_S) on pseudo-C_3 axis for $\Delta_R\Lambda_S$-$[Ir_2(aet)_4(cysta)]^{2+}$, while the oblique conformations (δ for Δ_R; λ for Δ_S) for the rhodium complex, although all of the other chelate rings take only the oblique conformations on the pseudo-C_3 axis. These seem to indicate that the oblique conformations are more favorable in $\Delta_R\Lambda_S$-$[M_2(aet)_4(cysta)]^{2+}$ than the parallel ones.

3-3-2. Characterization

The ^{13}C NMR spectra are shown in Figure 3-3, and the chemical shifts of $\Delta_R\Lambda_S$-$[M_2(aet)_4(cysta)]^{2+}$ (M = Ir^{III} (**3**), Rh^{III} (**4**)) are listed in Table 3-6, together with some other related polynuclear complexes. Each of **3** and **4** exhibits six signals due to the twelve methylene carbon atoms of the aet and cysta ligands because of the *meso* form. They are divided into three kinds of groups, that is, two signals (δ, 52 - 55) at the lower field, two signals (δ, 45 - 48) at the middle field, and two signals (δ, 29 - 34) at the higher field. The trinuclear $[Co\{M(aet)_3\}_2]^{3+}$ complexes, which also have the twelve methylene carbon atoms of the aet ligands, exhibit only two signals due to two kinds of methylene carbon atoms, and they have been assignable that the signal (δ, 49 - 52) at the lower field is due to the carbon atoms adjacent to the amino group and another signal (δ, 33 - 35) at the higher field is due to those to the bridging sulfur atoms.[2,3] Similar trends were also observed for the T-cage-type polynuclear complexes (δ, 51 - 53 and 33 - 35; Table 3-6).[4,5] On the other hand, the ^{13}C NMR spectra of $[Cu_4\{M(aet)_3\}_2\{M_2(aet)_4(cysta)\}]^{6+}$ (M =

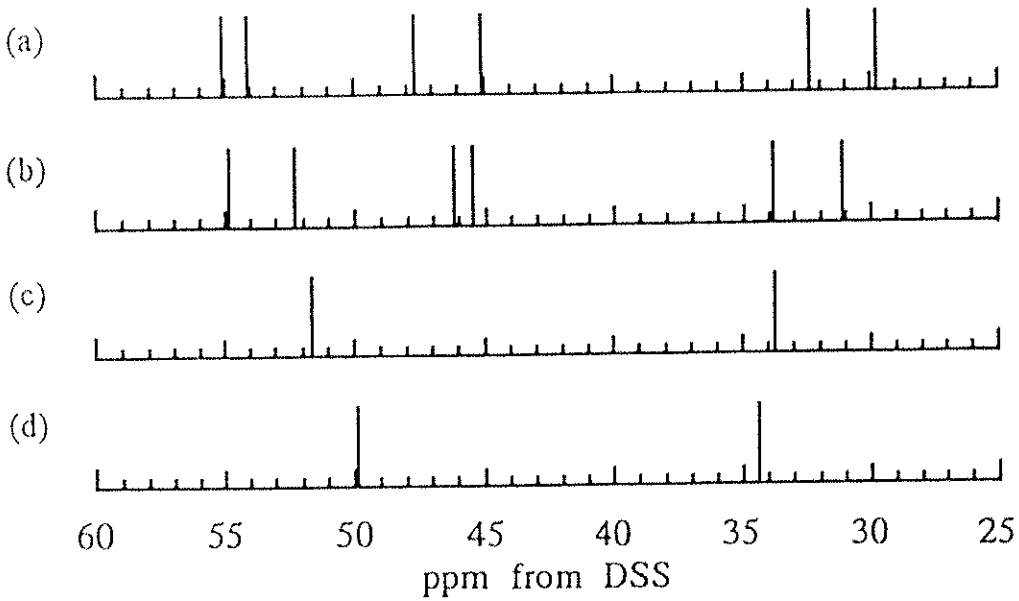

Figure 3-3. ^{13}C NMR spectra of (a) $\Delta_R\Lambda_S$-$[Ir_2(aet)_4(cysta)]^{2+}$, (b) $\Delta_R\Lambda_S$-$[Rh_2(aet)_4(cysta)]^{2+}$, (c) $\Delta\Lambda$-$[Co\{Ir(aet)_3\}_2]^{3+}$, and (d) $\Delta\Lambda$-$[Co\{Rh(aet)_3\}_2]^{3+}$ in D_2O.

Table 3-6. ^{13}C NMR Chemical Shifts[a] of $[M_2(aet)_4(cysta)]^{2+}$ and Its Related Complexes

Complexes	aet NH_2-CH_2	cysta NH_2-CH_2	cysta S-CH_2	aet S-CH_2
$\Delta_R\Lambda_S$-$[Ir_2(aet)_4(cysta)]^{2+}$ (3)	55.11 54.11	47.66	45.11	32.36 29.77
$\Delta_R\Lambda_S$-$[Rh_2(aet)_4(cysta)]^{2+}$ (4)	54.85 52.33	46.20	45.50	33.83 31.14
$\Delta\Lambda$-$[Co\{Ir(aet)_3\}_2]^{3+}$ [b]	51.64			33.74
$\Delta\Lambda$-$[Co\{Rh(aet)_3\}_2]^{3+}$ [c]	49.89			34.40
$[Zn_4O\{Ir(aet)_3\}_4]^{6+}$ [d]	52.69			33.36
$[Zn_4O\{Rh(aet)_3\}_4]^{6+}$ [e]	51.20			33.86
$[Cu_4\{Ir(aet)_3\}_2\{Ir_2(aet)_4(cysta)\}]^{6+}$ [f,g]	54.09 53.53 53.04 52.88	48.51 47.14	44.20 43.39	35.72 35.06 34.55
$[Cu_4\{Ir(aet)_3\}_2\{Rh_2(aet)_4(cysta)\}]^{6+}$ [f,g]	53.76 51.68 51.24 51.07	46.96	45.06 44.63	36.79 35.93

a) In ppm from DSS. b) Ref. 2. c) Ref. 3. d) Ref. 5. e) Ref. 4. f) Ref. 9. g) These complexes have three different types of sulfur atoms, μ_2- and μ_3-thiolato and disulfide. Accordingly, assignments of signals are not clearly.

Ir^{III} and Rh^{III}), which contain not only the aet ligands but also the cysta ligand with the coordinated disulfide, exhibit several additional signals (δ, 43 - 49) at middle field and the other two kinds of groups (δ, 51 - 54 and 34 - 37). These facts suggest that the signals due to methylene carbon atoms of the cysta ligand with the disulfide bond would appear in this middle field region, and the other signals at the lower and higher fields are also due to the methylene carbon atoms for the aet ligands. In addition, it is noted in the present dinuclear complexes, $[Co\{M(aet)_3\}_2]^{3+}$,[2,3] $[Zn_4O\{M(aet)_3\}_4]^{3+}$,[4,5] and $[Cu_4\{M(aet)_3\}_2\{M_2(aet)_4(cysta)\}]^{6+}$ [9] (M = Ir^{III} and Rh^{III}) that the chemical

shifts of the aet ligand in the iridium complexes are more separated than those of the rhodium complexes (Table 3-6). It supports that three signals at lower field and three signals at higher field, respectively, are assigned to the methylene carbon atoms adjacent to the amino group and those to the sulfur atom.

The electronic absorption spectra of $[M_2(aet)_4(cysta)]^{2+}$ (M = Ir^{III} (**3**), Rh^{III} (**4**)), are shown in Figures 3-4 and 3-5, together with the corresponding *fac(S)*-[M(L-cys-*N*,*S*)$_3$]$^{3-}$. The diffuse reflectance as well as absorption spectral data are summarized in Table 3-7. The absorption spectrum of $[Ir_2(aet)_4(cysta)]^{2+}$ is quite similar to that of 2 mol of *fac(S)*-[Ir(L-cys-*N*,*S*)$_3$]$^{3-}$ at the high energy region, which exhibits two spin-allowed d-d transition bands

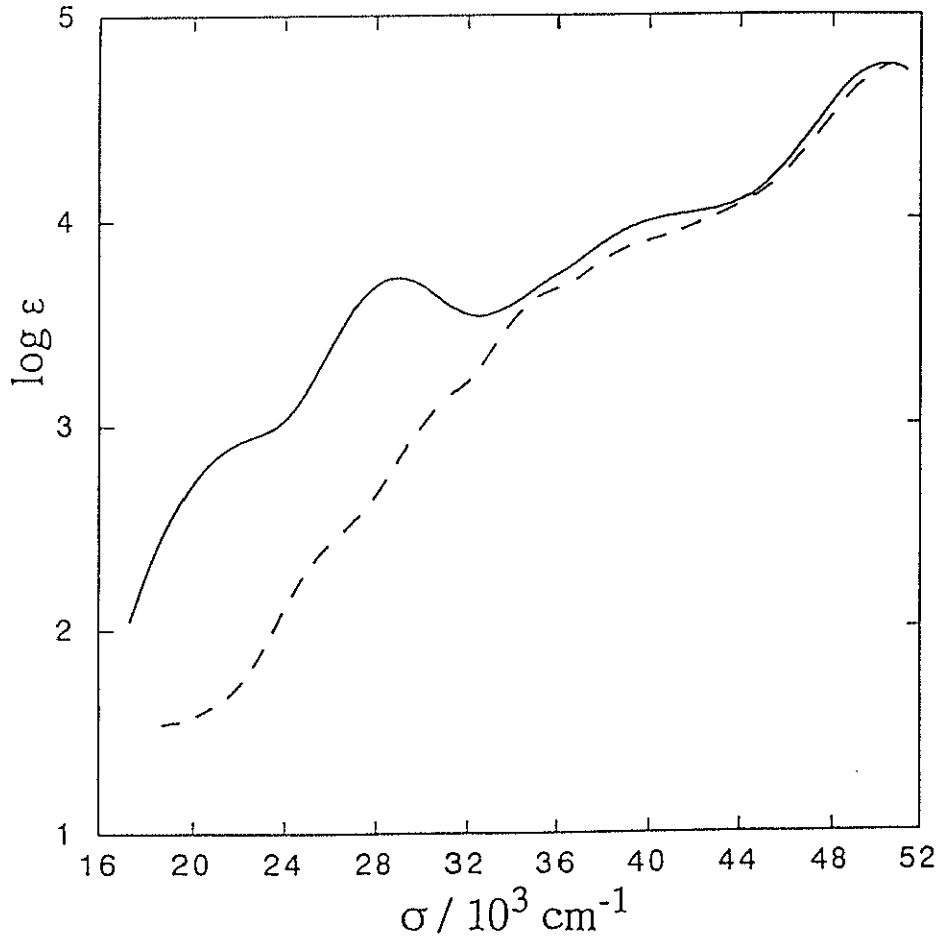

Figure 3-4. Electronic absorption spectra of $\Delta_R\Lambda_S$-$[Ir_2(aet)_4(cysta)]^{2+}$ (**3**; ————) and *fac(S)*-[Ir(L-cys-*N*,*S*)$_3$]$^{3-}$ (– – – –).

at ca. 32 - 41 x 10^3 cm^{-1} and the sulfur-to-iridium charge transfer band at ca. 50 x 10^3 cm^{-1} (Figure 3-4 and Table 3-7).[2] A similar trend was observed for the corresponding rhodium complexes (25 - 32 x 10^3 cm^{-1} for d-d transition; ca. 43 x 10^3 cm^{-1} for sulfur-to-rhodium charge transfer transition; Figure 3-5 and Table 3-7).[4] This absorption spectral behavior was also observed for the T-cage-type polynuclear complexes,[4-8] in which the Zn^{2+}, Cd^{2+} and Hg^{2+} metals take the d^{10} electron states, and their complexes are almost colorless. In contrast with these polynuclear complexes, the present dinuclear complexes $[M_2(aet)_4(cysta)]^{2+}$ are orange, and their absorption bands are intensified in the visible and near-ultraviolet regions (< ca. 32 x 10^3 cm^{-1} for Ir complex; < ca. 25 x 10^3 cm^{-1} for Rh complex). This seems to depend on the fact that the

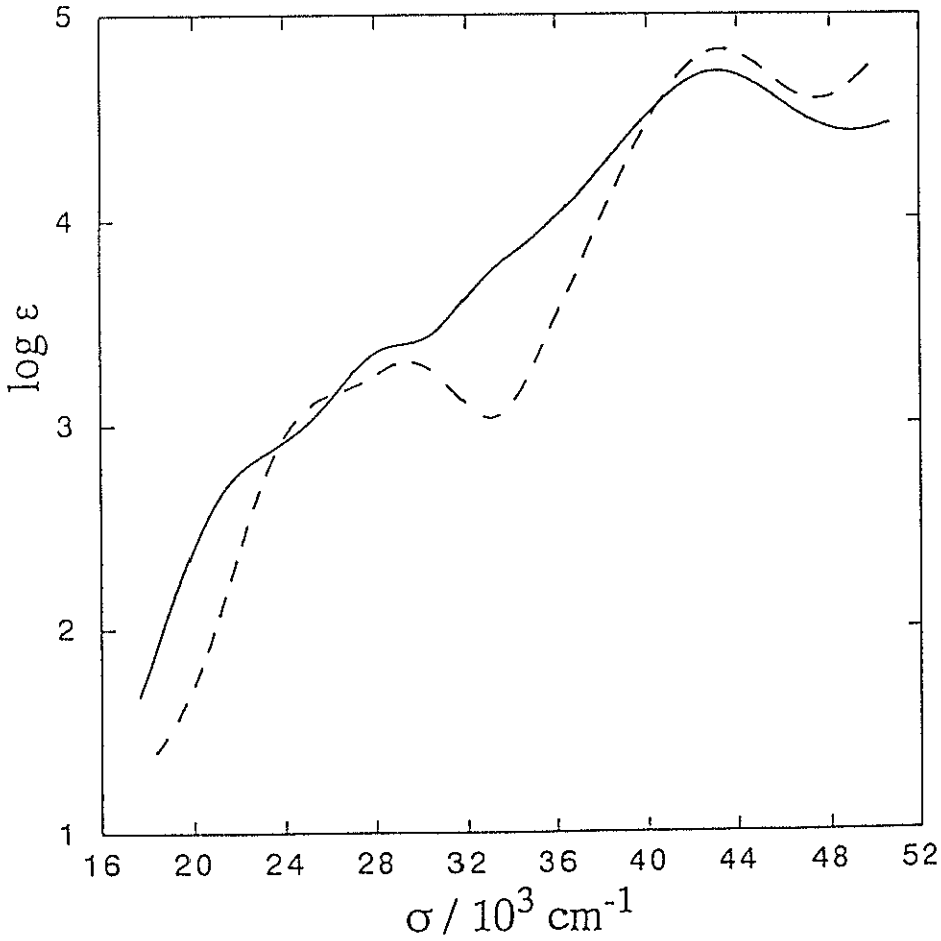

Figure 3-5. Electronic absorption spectra of $\Delta_R\Lambda_S$-$[Rh_2(aet)_4(cysta)]^{2+}$ (**4**; ———) and *fac(S)*-$[Rh(L\text{-}cys\text{-}N,S)_3]^{3-}$ (– – – –).

Table 3-7. Electronic Absorption and Diffuse Reflectance Spectral Data of $[M_2(aet)_4(cysta)]^{2+}$ and Its Related Complexes

Complexes	Absorption maxima σ / 10^3 cm^{-1} (log ε / mol^{-1} dm^3 cm^{-1})	Reflectance maxima σ / 10^3 cm^{-1}
$[Ir_2(aet)_4(cysta)]^{2+}$ (**3**)	22.0 (2.9sh [a)]) 29.07 (3.72) 35.5 (3.7sh) 40.8 (4.0sh) 50.63 (4.76)	21.7sh 27.8 39.8sh
$[Rh_2(aet)_4(cysta)]^{2+}$ (**4**)	22.4 (2.8sh) 29.1 (3.4sh) 33.9 (3.8sh) 43.10 (4.72)	20.3sh 26.1 29.9 40.8sh
fac(S)-[Ir(L-cys-*N*,*S*)$_3$]$^{3-}$ [b)]	27.8 (3.3sh) 31.7 (2.9sh) 36.0 (3.4sh) 41.3 (3.7sh) 50.76 (4.45)	
fac(S)-[Rh(L-cys-*N*,*S*)$_3$]$^{3-}$ [c)]	26.3 (2.9sh) 29.59 (3.05) 43.48 (4.61)	
fac(S)-[Ir(aet)$_3$]		25.1sh 31.3 34.8 38.7
fac(S)-[Rh(aet)$_3$] [c)]	26.3 (2.9sh) 30.03 (3.10) 44.05 (4.59)	25.4 28.7sh 34.8 44.6sh
fac(S)-[Ir(aesi)$_3$] [d)]		35.1sh 41.0 46.1sh
fac(S)-[Rh(aesi)$_3$] [d)]		30.3sh 34.8 45.0

a) sh denotes a shoulder. b) Ref. 2. c) Ref. 4.
d) These complexes are sparingly soluble in any solvent.

thiolato sulfur atoms, which coordinated to the iridium or rhodium atom, are oxidized to form the disulfide bond. The absorption bands of $[Rh_2(aet)_4(cysta)]^{2+}$ in this region are significantly smaller intensification than the corresponding iridium complex (Figures 3-4 and 3-5). Considering the M-S distances of the disulfide group and the thiolate groups, which are determined by the crystal structural analyses, it seems that the intensified bands in the visible and near-ultraviolet regions highly depend upon the shorter M-S distances of the disulfide group than the usual ones and would be dominated by the sulfur-to-metal charge transfer transitions.[13] Namely, the M-S distances in the iridium complex is much shorter than that of the rhodium complex. In addition, the characteristic intense bands of diffuse reflectance spectra of **3** and **4** are observed at similar region to the bands of absorption spectra in water (Table 3-7). This result also supports that the structures of **3** and **4** in solid state retain the dinuclear structure in solution. Moreover, the absorption spectra change little at least for several hours. Taking account of the absorption spectral, the ^{13}C NMR spectral, and the molar conductivity behavior, it seems to be indicated that $\Delta_R\Lambda_S$-$[M_2(aet)_4(cysta)]^{2+}$ are fairly stable in solution, and the disulfide-bridged dinuclear structure observed in crystals are retained in their aqueous solution.

The infrared spectra of $[M_2(aet)_4(cysta)]^{2+}$ ($M = Ir^{III}$ (**3**), Rh^{III} (**4**)) and corresponding *fac(S)*-$[M(aet)_3]$ are shown in Figure 3-6. The infrared and Raman spectral data of these complexes and *fac(S)*-$[M(aesi)_3]$ are listed in Table 3-8. The infrared spectral pattern of $[M_2(aet)_4(cysta)]^{2+}$ and *fac(S)*-$[M(aet)_3]$ are coincident with each other in the region of 1000 - 400 cm^{-1}, although slight shifts are observed (Figure 3-6 and Table 3-8). In the region near 570 cm^{-1}, however, the characteristic bands (573 cm^{-1} for **3**; 571 cm^{-1} for **4**) are appeared in $[M_2(aet)_4(cysta)]^{2+}$ but not in *fac(S)*-$[M(aet)_3]$. Similarly, in the Raman spectra, the characteristic bands (641 cm^{-1} for **3**; 637 cm^{-1} for **4**) in the region near 640 cm^{-1} is appeared in $[M_2(aet)_4(cysta)]^{2+}$ but not in *fac(S)*-$[M(aet)_3]$ (Table 3-8). It was reported that the ν(S-S) bands of the vibrational spectra were observed in the range from ca. 600 to 480 cm^{-1} for the disulfide complexes.[13] No significant spectral difference of the dinuclear complexes

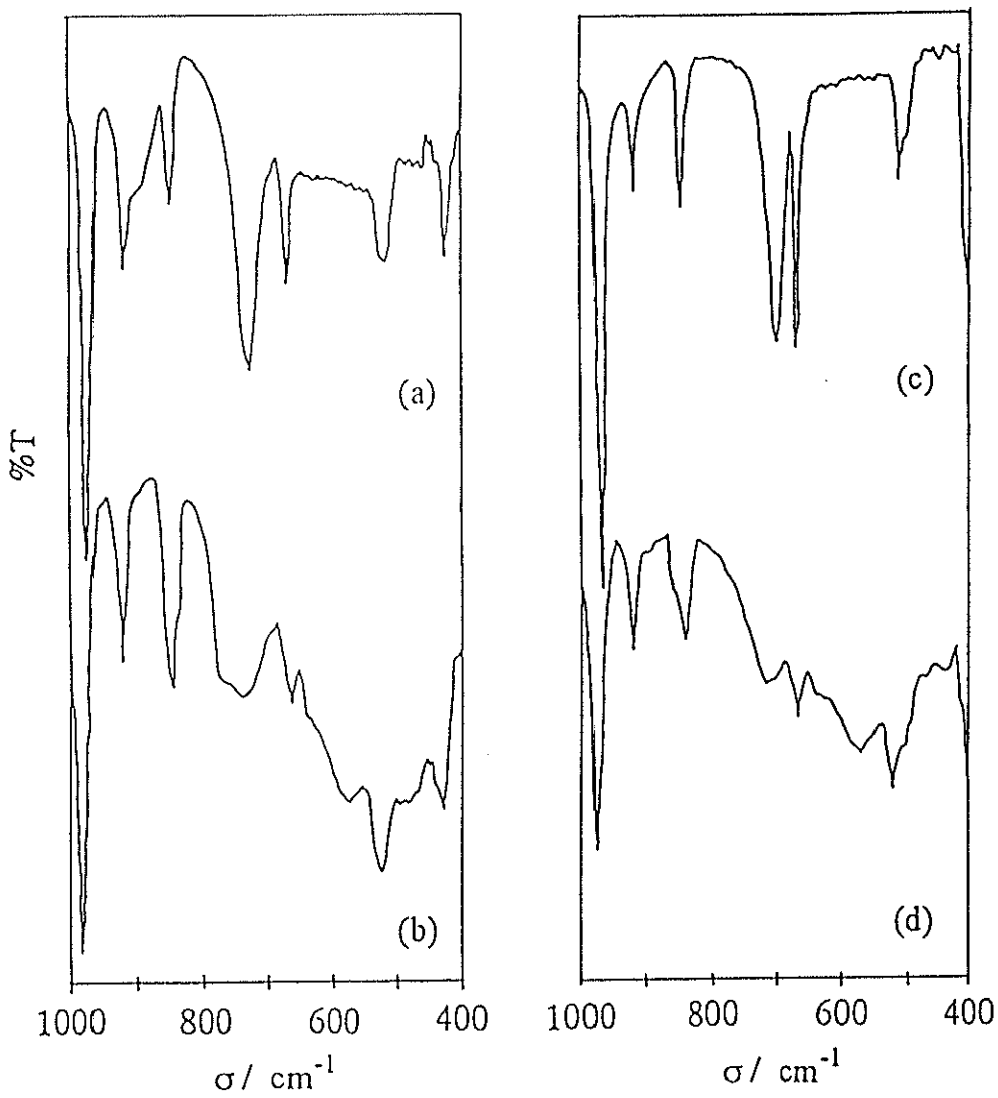

Figure 3-6. Infrared spectra of (a) *fac(S)*-[Ir(aet)$_3$], (b) [Ir$_2$(aet)$_4$(cysta)]$^{2+}$, (c) *fac(S)*-[Rh(aet)$_3$], and (d) [Rh$_2$(aet)$_4$(cysta)]$^{2+}$.

are caused by the difference of the iridium(III) and rhodium(III) ions. Accordingly, it can be assigned that the characteristic bands for infrared and Raman spectra are due to the disulfide bond coordinated to the metal ions. In addition, the infrared spectra of *fac(S)*-[M(aesi)$_3$] exhibit characteristic intense bands at 1190 and 1049 cm^{-1} for iridium complex and at 1194 and 1049 cm^{-1} for rhodium complex (Table 3-8). It has reported that the S-O distances are characteristically longer for the sulfenato moieties (average 1.55 Å) than the sulfinato moieties (average 1.46 Å). The S-O distances correlate with infrared data in the ν(S-O) region; the shorter bonds of the sulfinato moieties

(SO_2) result in characteristic infrared bands at ca. 1200 and 1050 cm^{-1}, while the sulfinato moieties (SO) are in the 925 - 910 cm^{-1} range.[24] The single set of signals, which attributed to the symmetric stretching vibration mode of $\nu(SO_2)$, of *fac(S)*-[M(aesi)$_3$] implies three equivalent sulfinato in the complexes.

Table 3-8. Infrared and Raman Spectral Data of $[M_2(aet)_4(cysta)]^{2+}$ and Its Related Complexes

Complexes	peak σ / cm^{-1}
$[Ir_2(aet)_4(cysta)]^{2+}$ (3)	
Infrared spectra	3391br 3198vs 3117vs 2954m 2925s 2871w 1620s 1589vs 1451m 1433w 1412w 1383w 1311w 1276m 1244m 1156s 1109m 1040m 983s 920m 845m 743w 659w 573br 524m 428w
Raman spectra	1656w 1477w 1456w 1438w 1317w 1163w 1113w 1046w 993w 925w 855w 848w 673m 664m 641m 522m 507 455s 439w 420vs 375s 362s 308w 285w 264m 245m 173w
$[Rh_2(aet)_4(cysta)]^{2+}$ (4)	
Infrared spectra	3461br 3313w 3215vs 3210s 2952m 2924s 2860w 1631s 1583vs 1450m 1422w 1406w 1387w 1299w 1276m 1231m 1130m 1101m 1046m 975s 922m 845m 718w 666w 571br 522m 403w
Raman spectra	1580w 1460w 1440w 1426w 1321w 1303w 1166w 1126w 1103w 1046w 997w 929w 864w 852w 675m 666w 637m 513m 502w 444s 408s 373vs 353s 306m 277s 240s 223s 204s 185m
fac(S)-[Ir(aet)$_3$]	
Infrared spectra	3434br 3248vs 3166vs 3082w 2921s 2857m 2818w 1631w 1571m 1449m 1421m 1371w 1295m 1277w 1231w 1132m 1095m 1043m 975s 917w 848w 726m 666w 515w 423w
Raman spectra	1655w 1579w 1557w 1455w 1428w 1422w 1372w 1298w 1280w 1233w 1135w 1098w 1047w 980m 922m 852m 727w 673s 519w 449s 428m 348s 299w 263w 243vs 202s 162m

Table 3-8. Continued.

Complexes	peak σ / cm^{-1}
fac(S)-[$Rh(aet)_3$]	
Infrared spectra	3437br 3274vs 3169vs 3076w 2902s 2851m 2817w 1631w 1570m 1448m 1419w 1369w 1289w 1271m 1224w 1109w 1087m 1044s 968s 918w 847w 696m 666m 511w 497w 404m
Raman spectra	1565w 1455w 1432w 1419w 1370w 1292w 1277w 1224w 1113w 1093w 1049w 974m 923m 851m 692w 673s 503w 429s 409m 347s 304w 267m 231vs 188s 165m
fac(S)-[$Ir(aesi)_3$]	
Infrared spectra	3452br 3257vs 3212vs 2993w 2972w 2853w 1641w 1577w 1462w 1397m 1259m 1190vs 1153s 1106s 1049vs 989m 925w 862w 763w 699m 569w 554m 524w 465s
fac(S)-[$Rh(aesi)_3$]	
Infrared spectra	3452br 3276vs 3227vs 3142w 2987w 2967w 2851w 1641w 1574w 1562w 1459w 1394m 1246m 1194vs 1136s 1098s 1049vs 983s 944w 927w 860w 737w 720w 689m 563w 550m 514m 453s 415w

3-3-3. Formation of Disulfide Bond

The reaction of *fac(S)*-[$Ir(aet)_3$] with a large excess of acid (1 mol dm^{-3} HCl solution) in water gave the dinuclear complex, $\Delta_R\Lambda_S$-$[Ir_2(aet)_4(cysta)]^{2+}$. In this reaction, the oxidation is proceeded by the acid. This is supported by the results that the same dinuclear complexes was also obtained by the reactions of *fac(S)*-[$Ir(aet)_3$] with 0.15 mol dm^{-3} HNO_3 solution or $Cr(NO_3)_3 \cdot 9H_2O$, whose aqueous solution is acid condition. In contrast to the iridium dinuclear complexes, $[Rh_2(aet)_4(cysta)]^{2+}$ are hardly formed by a procedure similar to that for the acid solution (1 mol dm^{-3} HCl), using *fac(S)*-[$Rh(aet)_3$]. Although the reaction of *fac(S)*-[$Ir(aet)_3$] with chromium(III) ion was accompanied by the dinuclear iridium complex, the reaction of *fac(S)*-

$[Rh(aet)_3]$ was accompanied by the unidentified rhodium complex (chapter 2). $[Rh_2(aet)_4(cysta)]^{2+}$ are formed by the reaction with an equivalent strong oxidizing agent of $K_2Cr_2O_7$ or $Ce(SO_4)_2$. Although *meso*- and *rac*-$[Fe\{Rh(aet)_3\}_2]^{3+}$ were prepared by the reaction of $FeCl_3$ with *fac(S)*-$[Rh(aet)_3]$,[25] the corresponding $[Fe\{Ir(aet)_3\}_2]^{3+}$ has not been obtained by the reaction of $FeCl_3$ with *fac(S)*-$[Ir(aet)_3]$. In this system, iron(III) ion may be reduced to iron(II) ion by *fac(S)*-$[Ir(aet)_3]$, and $[Ir_2(aet)_4(cysta)]^{2+}$ was formed only. In fact, the cyclic voltammetry experiments in 1 mol dm^{-3} HCl solution indicated that oxidation waves of *fac(S)*-$[Ir(aet)_3]$ (E_{pa} = + 0.37 and + 0.55 V) observed at more negative potential region than those of corresponding rhodium complex (E_{pa} = + 0.63 and + 0.75 V). Additionally, *meso*- and *rac*-$[Fe\{Co(aet)_3\}_2]^{3+}$ were also prepared by the reaction of iron(III) ion with *fac(S)*-$[Co(aet)_3]$.[26] These coincide well with the fact that *fac(S)*-$[Ir(aet)_3]$ would be oxidized more easily than *fac(S)*-$[Rh(aet)_3]$ and *fac(S)*-$[Co(aet)_3]$ to form the disulfide bonds.

As shown in Figure 3-7, each ^{13}C NMR spectrum of *fac(S)*-$[Ir(aet)_3]$ and *fac(S)*-$[Rh(aet)_3]$ in 1 mol dm^{-3} DCl exhibits only two signals (δ = 53.04 and 32.58 ppm for Ir complex; δ = 51.58 and 33.16 ppm for Rh complex) due to the aet ligands. $[Ir_2(aet)_4(cysta)]^{2+}$ is precipitated as a crystalline powder, and its signals are not appeared because of poor solubility in acid condition. On the other hand, corresponding $[Rh_2(aet)_4(cysta)]^{2+}$ is not formed even when the sample was allowed to stand for a week at room temperature. When the reaction mixture of *fac(S)*-$[Rh(aet)_3]$ was heated at 70 °C for 2h, the ^{13}C NMR signals appeared at the field of free ligands.[27] A similar dissociation reaction of the aet ligands was not observed in the case of *fac(S)*-$[Ir(aet)_3]$, and the *fac(S)*-$[Ir(aet)_3]$ units in the dinuclear complex are relatively stable to heat and oxidized by the acid, retaining the structure. These seem to indicate that the Rh-S bonds in acid solution are snapped before forming of the disulfide bonds. Accordingly, the Rh-S bonds in the *fac(S)*-$[Rh(aet)_3]$ units are weaker than the corresponding Ir-S bonds, and this result is in agreement with the experimental fact that strong oxidizing agents were required for preparing $[Rh_2(aet)_4(cysta)]^{2+}$. On the other hand, the treatment of *fac(S)*-$[Co(aet)_3]$ with 1 mol dm^{-3} DCl indicated the signals due to the *meso*- and *rac*-

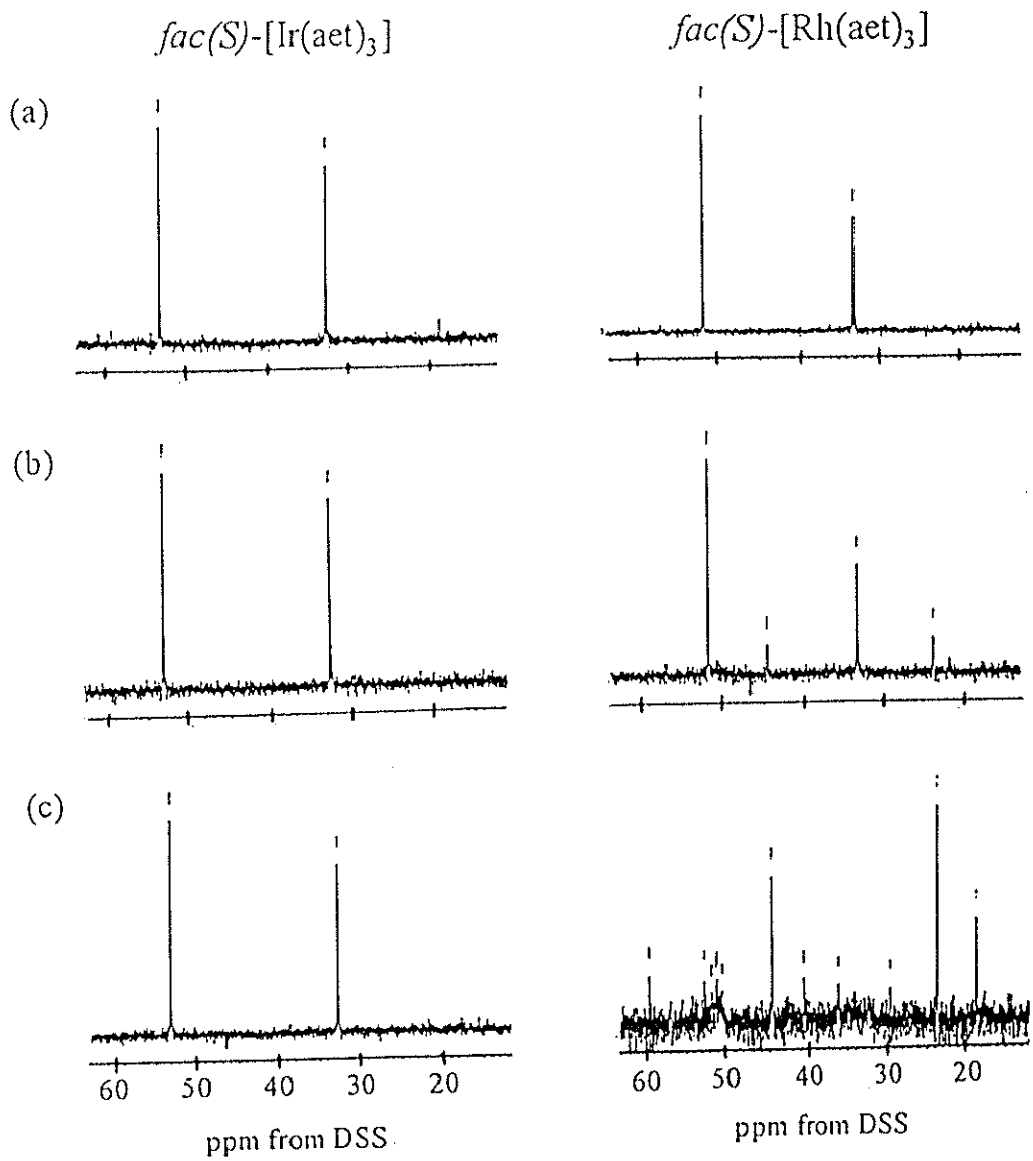

Figure 3-7. ^{13}C NMR spectral changes of *fac(S)*-$[M(aet)_3]$ in 1 mol dm^{-3} DCl; (a) 0 h, (b) stood at room temperature for 1 week, and (c) heated at 70 °C for 2 h.

$[Co\{Co(aet)_3\}_2]^{3+}$ [28] and free aet without heating. Although using the strong oxidizing agent, corresponding dinuclear cobalt complex was not obtained. Attempts to prepare the corresponding dinuclear chromium complex by the reaction of any oxidizing agents with *fac(S)*-$[Cr(aet)_3]$ were also not successful.

In order to elucidate the formation mechanism of $[Ir_2(aet)_4(cysta)]^{2+}$ (3) by the reaction of *fac(S)*-$[Ir(aet)_3]$ with chromium(III) ion, the changes with times of trinuclear complex, $[Cr\{Ir(aet)_3\}_2]^{3+}$, were determined by the column

chromatographic technique and the absorption spectral measurements, under acidic condition of 1 mol dm^{-3} HCl solution. Since the meso and racemic isomers exhibit a quite similar stability to each other (chapter 2), representative *meso*-isomer (1a) was used. Plots of the result of the existences of 1a and 3 calculated from absorbance at 385 and 342 nm, respectively, are shown in Figure 3-8. The existences of the $Ir^{III}Cr^{III}Ir^{III}$ trinuclear complexes gradually decrease, while those of the $Ir^{III}Ir^{III}$ dinuclear complex, $[Ir_2(aet)_4(cysta)]^{2+}$, increase more complicatedly. The spectral changes in $[Cr\{Ir(aet)_3\}_2]^{3+}$ mainly involve the decrease of the intense bands,

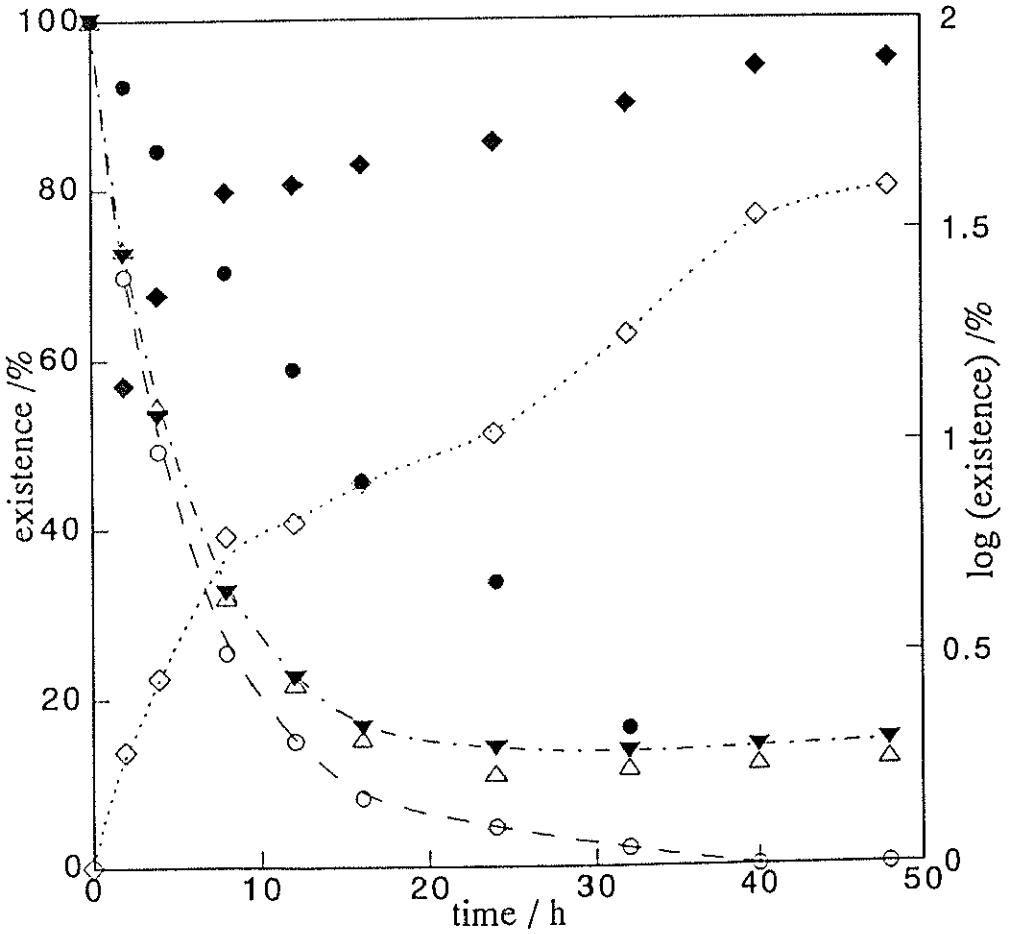

Figure 3-8. Changes with times of $\Delta\Lambda$-$[Cr\{Ir(aet)_3\}_2]^{3+}$ (1a); chromatographic technique, $[Cr\{Ir(aet)_3\}_2]^{3+}$ (○) and $[Ir_2(aet)_4(cysta)]^{2+}$ (3) (◇); absorbance changes at 385 nm, calculation values of $\varepsilon([Cr\{Ir(aet)_3\}_2]^{3+}) + \varepsilon([Ir_2(aet)_4(cysta)]^{2+})$ (▼) and measurements (△). Plots of log(existence) *versus* time; $[Cr\{Ir(aet)_3\}_2]^{3+}$ (●) and $[Ir_2(aet)_4(cysta)]^{2+}$ (◆).

which are assigned as arising from the central $Cr^{III}S_6$ chromophore (chapter 2). The $Ir^{III}Cr^{III}Ir^{III}$ complex exhibits its absorption peak at 25.97 x 10^3 cm^{-1} (chapter 2) and the $Ir^{III}Ir^{III}$ complex also shows the high absorbance at its wavelength (Figure 3-4). The absorbances calculated from the ratio of the $Ir^{III}Cr^{III}Ir^{III}$ and the $Ir^{III}Ir^{III}$ complexes, which were determined by the column chromatography, coincide well with those measured from the reaction mixture at 25.97 x 10^3 cm^{-1} (Figure 3-8). These mean that the unidentified compounds exhibit no significant absorbances in this region, indicating that they would involve the mononuclear iridium and chromium complexes or ions. Further, the plots of log(existence) versus times for the $Ir^{III}Cr^{III}Ir^{III}$ trinuclear and $Ir^{III}Ir^{III}$ dinuclear complexes seem to indicate that although the $Ir^{III}Cr^{III}Ir^{III}$ trinuclear complex is gradually decomposed, its decomposition is inhibited by an increase of the chromium(III) ion (Figure 3-8). Since the $Ir^{III}Ir^{III}$ complex is formed in spite of the absence of the $Ir^{III}Cr^{III}Ir^{III}$ trinuclear complex, the $Ir^{III}Ir^{III}$ complex seems to be rearranged from the decomposition compounds.

As described in chapter 2, the formation of the S-bridged trinuclear complexes, $[Cr^{III}\{M(aet)_3\}_2]^{3+}$ (M = Ir^{III} and Rh^{III}), which incorporate chromium(III) ion, required a large excess of chromium(III) ion and heating (Scheme 3-1). This difficulty in the formation of the trinuclear complexes would be due to the strong affinity of chromium(III) ion toward water oxygen atoms and the weak chromium-sulfur bonds. In the reaction, the dinuclear iridium complex, $[Ir_2(aet)_4(cysta)]^{2+}$, which does not involve chromium(III) ion, was also obtained, while corresponding dinuclear rhodium(III) complex was not formed by the similar reaction condition (Scheme 3-1). Considering the reactivity of the mononuclear and trinuclear complexes, additional reasons of difficulty in the formation of the trinuclear complexes were elucidated. Namely, the thiolato sulfur atoms of *fac(S)*-$[Ir(aet)_3]$ are oxidized and the aet ligands of *fac(S)*-$[Rh(aet)_3]$ are partially dissociated in the synthesis of the $MCr^{III}M$ complexes. Since the aet ligands of *fac(S)*-$[Co(aet)_3]$ are dissociate more easily than those of the rhodium or iridium complexes, both of the corresponding trinuclear $Co^{III}Cr^{III}Co^{III}$ and dinuclear $Co^{III}Co^{III}$ complexes could not formed.

Scheme 3-1.

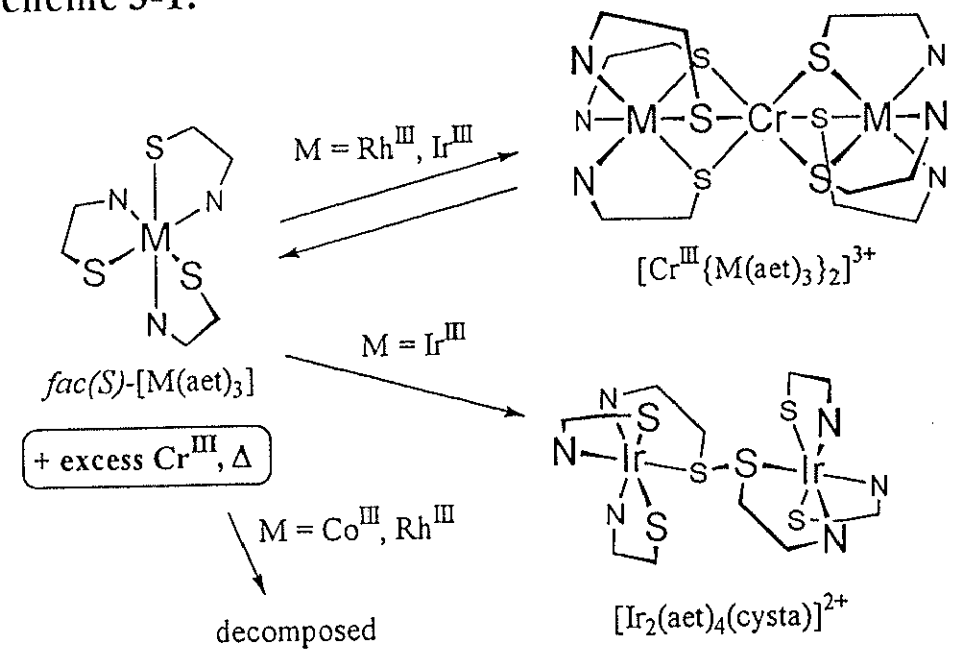

3-3-4. Electrochemistry and Reactivity

Electrochemical studies were performed for $[M_2(aet)_4(cysta)]^{2+}$ (M = Ir^{III} (**3**), Rh^{III} (**4**)) complexes in 0.1 mol dm^{-3} sodium sulfate aqueous solutions. As shown in Figure 3-9, the cyclic voltammograms at a glassy-carbon electrode for both **3** and **4** display an irreversible oxidation waves at a positive potential region and an irreversible reduction wave at a negative potential region. It seems to be indicated that the irreversible oxidation wave (E_{pa} = + 0.60 V) for **3** involves the terminal Ir(III)/Ir(IV) oxidation process, because the redox couples for the Ir(III)/Ir(IV) redox process of $[M'\{Ir(aet)_3\}_2]^{3+}$ (M' = Cr^{III} and Co^{III}) are appeared at a similar positive region (chapter 2). Similarly, the irreversible oxidation wave (E_{pa} = + 0.77 V) for **4** would involve the terminal Rh(III)/Rh(IV) oxidation process, because the redox couples are appeared at a similar positive region to the corresponding rhodium complexes (chapter 2). Therefore, these suggest that **3** is easily oxidized than **4**. The irreversible reduction waves (E_{pc} = - 0.63 V) for **3** appear at almost the same potential as that (E_{pc} = - 0.58 V) for **4**. Since it has been described in chapter 2 that the Ir(III)/Ir(II) and Rh(III)/Rh(II) redox process does not occur in the

potential region from + 1.1 to - 1.1 V for $[M'\{M(aet)_3\}_2]^{3+}$ ($M = Ir^{III}$, Rh^{III}; $M' = Cr^{III}$, Co^{III}), the irreversible reduction waves have probably influence on the cleavage of the disulfide bond. In fact, the addition of reducing agent such as $NaBH_4$ to the present dinuclear complexes gave the mononuclear thiolato complexes, *fac(S)*-$[M(aet)_3]$, in a quantitative yield (vide infra). The irreversible oxidation waves (E_{pa} = + 0.19 V for **3** and + 0.44 V for **4**) are not observed unless going through the reduction scans. This suggests that the dinuclear complexes are decomposed by the reduction process and the created species with the metal ions might be oxidized by the oxidation process. Similar oxidation waves were observed for $[M'\{M(aet)_3\}_2]^{3+}$ ($M = Ir^{III}$, Rh^{III}; $M' = Cr^{III}$, V^{III}).[21] Since only irreversible waves are observed about both of reduction and oxidation processes, it seems to be indicated that the dinuclear structures no longer exist in the redox process.

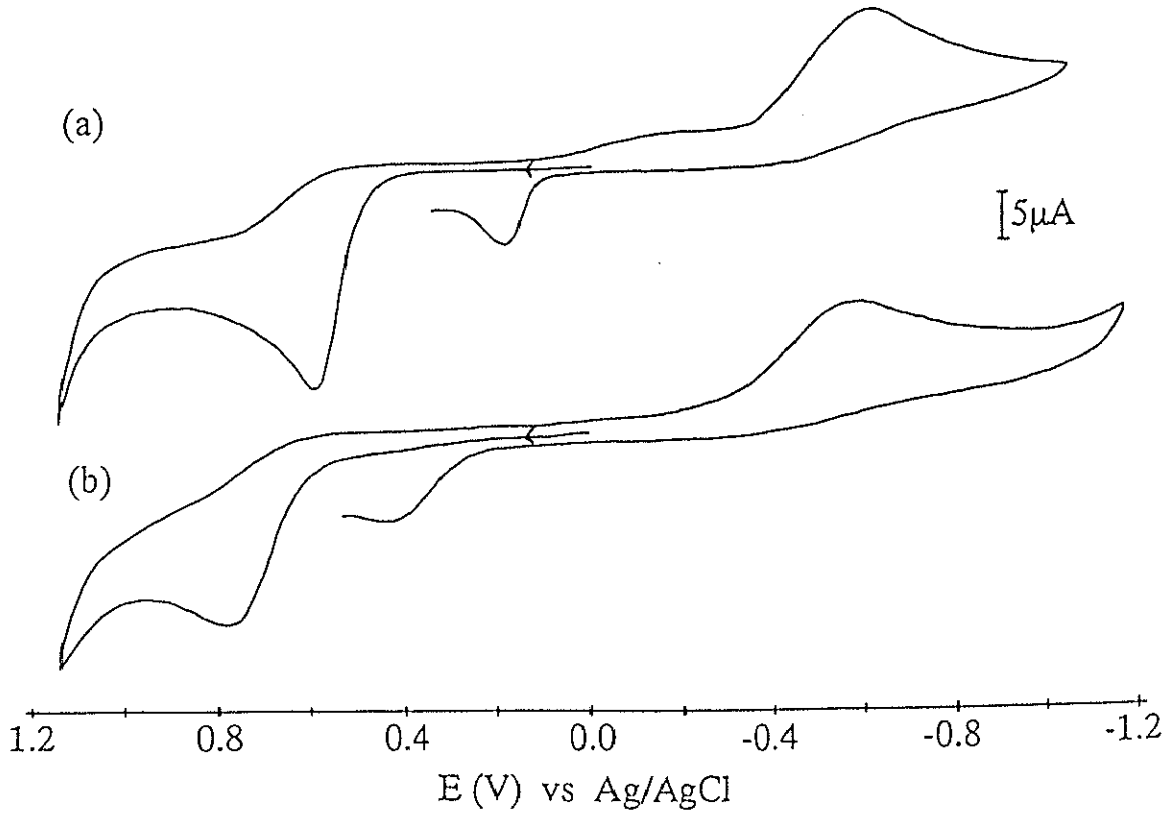

Figure 3-9. Cyclic voltammograms of $\Delta_R\Lambda_S$-$[M_2(aet)_4(cysta)]^{2+}$; (a) M = Ir and (b) M = Rh; scan rate 100 mV s^{-1}; in 0.1 mol dm^{-3} Na_2SO_4 aqueous solution.

In the present work, the novel dinuclear complexes, $[M_2(aet)_4(cysta)]^{2+}$ ($M = Ir^{III}$ and Rh^{III}), with a coordinated bridging disulfide bond, were formed by the oxidation reaction of *fac(S)*-$[M(aet)_3]$ (Scheme 3-2). These oxidation reactions were achieved by using equivalent strong oxidizing agents such as Ce^{4+}. In the case of the iridium complex, mild oxidizing agents such as acid also gave the intended dinuclear complex. When the dinuclear complexes were further oxidized using excess H_2O_2, the mononuclear sulfinato complexes, *fac(S)*-$[M(aesi)_3]$, were obtained (Scheme 3-2). This oxidation reaction reveals that the disulfide bonds are cleaved to form the sulfinato complexes. Taking account of the M-S and S-S distances for the disulfide bonds of $[M_2(aet)_4(cysta)]^{2+}$ ($M = Ir^{III}$ and Rh^{III}) in the crystal structural analysis, it is reasonable to assume that the disulfide bonds are cleaved, because the dinuclear structure is stereochemically labilized by the oxygen atoms, which would be bound to thiolato sulfur atoms by further oxidation reaction. Similar sulfinato complexes were also formed by the direct oxidation using H_2O_2 of the thiolato complexes (Scheme 3-2). *fac(S)*-$[Ir(aesi)_3]$ was newly prepared in this research, while *fac(S)*-$[Rh(aesi)_3]$,[11] *fac(S)*-$[Co(aesi)_3]$,[10] and *fac(S)*-$[Cr(aesi)_3]$[29] were previously obtained by the

Scheme 3-2.

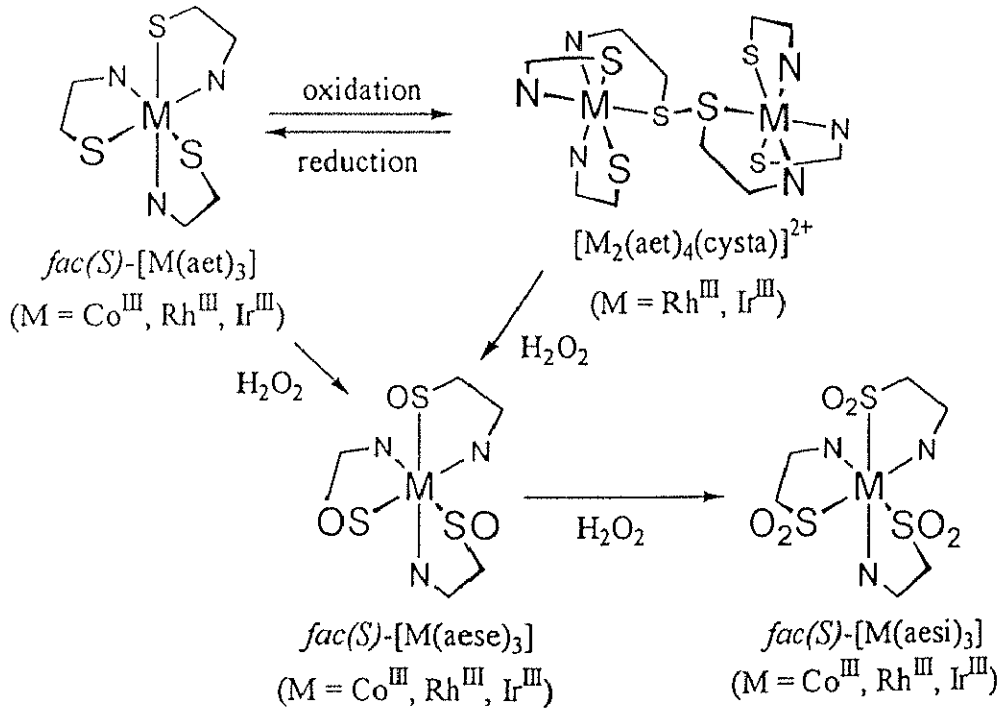

H_2O_2 oxidation reaction in an ice bath, probably because of preventing M-S bond cleavage. $[M_2(aet)_4(cysta)]^{2+}$, *fac(S)*-$[M(aese)_3]$, and *fac(S)*-$[M(aesi)_3]$ are formed by 1, 6, and 12 electron oxidation of *fac(S)*-$[M(aet)_3]$, respectively, and the present dinuclear complexes can be regarded as the intermediate. Although reduction of the sulfenato or sulfinato complexes is difficult, the addition of base such as NaOH or $NaBH_4$ to the aqueous solution of $[M_2(aet)_4(cysta)]^{2+}$ gave the white or yellow suspension was appeared immediately, from which starting *fac(S)*-$[M(aet)_3]$ were precipitated in a quantitative yield (Scheme 3-2). Thus, one of the functional interest is the fact that conversion of the coordinated thiolato to the coordinated bridging disulfide is reversible. It will be expected the dinuclear complexes, $[M_2(aet)_4(cysta)]^{2+}$, as oxidation agents.

Attempts to prepare a trinuclear complex, which is bounded between two thiolato sulfur atoms by Ag^+ and a dinuclear complex, which is bounded to thiolato sulfur atoms by the methyl group, retaining disulfide bond were not successful. Reaction mixture of $[Ir_2(aet)_4(cysta)]^{2+}$ with $AgNO_3$ or CH_3I was almost colorless, which implies S-S bond cleavage. Such chemical modification of the thiolato sulfur atoms also caused instabilization of the dinuclear structure. Additionally, reactions of $[Ir_2(aet)_4(cysta)]^{2+}$ with cobalt(II) or platinum(II) ion was attempted, and *meso*- and *rac*-$[M'\{Ir(aet)_3\}_2]^{n+}$ ($M' = Co^{III}$ and Pt^{IV}, respectively) were isolated by column chromatography.[30] In the reaction with platinum(II) ion, the white precipitate of *fac(S)*-$[Ir(aet)_3]$ was appeared immediately. On the other hand, *fac(S)*-$[Ir(aet)_3]$ may not form in the reaction with cobalt(II) ion. These S-bridged polynuclear complexes were also obtained by the reaction of *fac(S)*-$[Ir(aet)_3]$ with cobalt(III) or platinum(IV) ion. Considering the redox potential of cobalt(II) and platinum(II) ions, oxidation of cobalt(II) to cobalt(III) by *fac(S)*-$[Ir(aet)_3]$ would be difficult. It is reasonable to assume that the S-S bond cleavage occur after cobalt(II) ion bounds to the thiolato sulfur atoms of $[Ir_2(aet)_4(cysta)]^{2+}$, while it seems that S-S bond cleavage occur before platinum(II) ion bounds to the thiolato sulfur atoms. From these properties, the present dinuclear complex may be regarded as a building block, which have an oxidizing ability.

References and Notes

1) Y. Miyashita, N. Sakagami, Y. Yamada, T. Konno, J. Hidaka, and K. Okamoto, *Bull. Chem. Soc. Jpn.*, **71**, 661 (1998).

2) T. Konno, K. Nakamura, K. Okamoto, and J. Hidaka, *Bull. Chem. Soc. Jpn.*, **66**, 2582 (1993).

3) T. Konno, S. Aizawa, K. Okamoto, and J. Hidaka, *Bull. Chem. Soc. Jpn.*, **63**, 792 (1990).

4) T. Konno, K. Okamoto, and J. Hidaka, *Inorg. Chem.*, **33**, 538 (1994).

5) K. Okamoto, T. Konno, and J. Hidaka, *J. Chem. Soc., Dalton Trans.*, **1994**, 533.

6) a) T. Konno, K. Okamoto, and J. Hidaka, *Inorg. Chem.*, **30**, 2253 (1991); b) T. Konno, K. Okamoto, and J. Hidaka, *Chem. Lett.*, **1990**, 1043; c) T. Konno, K. Okamoto, and J. Hidaka, *Bull. Chem. Soc. Jpn.*, **67**, 101 (1994).

7) T. Konno, Y. Kageyama, and K. Okamoto, *Bull. Chem. Soc. Jpn.*, **67**, 1957 (1994).

8) a) K. Okamoto, T. Konno, Y. Kageyama, and J. Hidaka, *Chem. Lett.*, **1992**, 1105; b) K. Okamoto, Y. Kageyama, and T. Konno, *Bull. Chem. Soc. Jpn.*, **68**, 2573 (1995); c) Y. Kageyama, T. Konno, K. Okamoto, and J. Hidaka, *Inorg. Chim. Acta*, **239**, 19 (1995).

9) T. Konno, K. Okamoto, and J. Hidaka, *Inorg. Chem.*, **31**, 3875 (1992).

10) a) M. Kita, K. Yamanari, and Y. Shimura, *Chem. Lett.*, **1980**, 275; b) M. Kita, K. Yamanari, K. Kitahara, and Y. Shimura, *Bull. Chem. Soc. Jpn.*, **54**, 2995 (1981).

11) M. Kita, K. Yamanari, and Y. Shimura, *Bull. Chem. Soc. Jpn.*, **56**, 3272 (1983).

12 a) E. Deutsch, M. J. Root, and D. L. Nosco, *Adv. Inorg. Bioinorg. Mech.*, **1**, 269 (1982); b) P. J. Blower and J. R. Dilworth, *Coord. Chem. Rev.*, **76**, 121 (1987).

13) A. Müller, W. Jaegermann, and J. H. Enemark, *Coord. Chem. Rev.*, **46**, 245 (1982).

14) J. D. Lydon, R. C. Elder, and E. Deutsch, *Inorg. Chem.*, **21**, 3186 (1982).

15) M. Woods, J. Karbwang, J. C. Sullivan, and E. Deutsch, *Inorg. Chem.*, **15**,

1678 (1976).
16) M. J. Heeg, E. L. Blinn, and E. Deutsch, *Inorg. Chem.*, **24**, 1118 (1985).
17) In the synthesis of *fac(S)*-[Ir(L-cys-*N*,*S*)$_3$]$^{3-}$, the 'black' $IrCl_3$ was used. *fac(S)*-[Ir(L-cys-*N*,*S*)$_3$]$^{3-}$ could not isolated by using 'green' $IrCl_3$. The 'black' $IrCl_3$ was purchased from Wako Pure Chemical Ind., Co., Ltd.
18) Molecular Mechanics. Version 3.7. CAChe Scientific, Inc, 1994.
19) SIR92. A. Altomare, M. C. Burla, M. Camalli, M. Cascarano, C. Giacovazzo, A. Guagliardi, and G. Polidori, *J. Appl. Cryst.*, **27**, 435 (1994).
20) teXsan. Molecular Structure Corporation. Single Crystal Structure Analysis Software. Version 1.8, MSC, 3200 Research Forest Drive, The Woodlands, TX 77381, USA (1997).
21) unpublished data.
22) R. C. Elder, L. R. Florian, R. E. Lake, and A. M. Yacynych, *Inorg. Chem.*, **12**, 2690 (1973).
23) D. L. Nosco, R. C. Elder, and E. Deutsch, *Inorg. Chem.*, **19**, 2545 (1980).
24) C. A. Grapperhaus and M. Y. Darensbourg, *Acc. Chem. Res.*, **31**, 451 (1998).
25) S. Aizawa, *Ph. D. Thesis, University of Tsukuba*, **1989**.
26) G. Freeh, K. Chapman, and E. Blinn, *Inorg. Nucl. Chem. Lett.*, **9**, 91 (1973).
27) δ = 24.14 and 35.99 ppm for CH_2S, δ = 44.83 and 40.43 ppm for CH_2NH_2 of aet and cysta free ligands, respectively. According to the blank test using Haet, the signal at 18.70 ppm is due to a decomposed material.
28) K. Nakamura, *Master Thesis, University of Tsukuba*, **1993**.
29) M. Matsumoto, *Master Thesis, University of Tsukuba*, **1995**.
30) *meso*- and *rac*-[Pt^{IV}{Ir(aet)$_3$}$_2$]$^{4+}$ complexes have not been reported. Two brown bands were eluted with using a 0.4 mol dm^{-3} NaCl aqueous solution. These bands indicated similar absorption spectra each other. To the reaction mixture was added an excess NaBr aqueous solution, which gave light-brown powder. Found: C, 9.98; H, 3.24; N, 5.62 %. Calcd for [Pt{Ir(aet)$_3$}$_2$]Br$_4$·5H$_2$O = $C_{12}H_{36}N_6S_6Br_4Ir_2Pt$·5H$_2$O: C, 9.97; H, 3.21; N, 5.81 %.